DOI 10.1002/pmic.200600459

RESEARCH ARTICLE

Proteomic analysis of up-regulated proteins in human promonocyte cells expressing severe acute respiratory syndrome coronavirus 3C-like protease

Chien-Chen Lai[1, 2], Ming-Jia Jou[3], Shiuan-Yi Huang[1], Shih-Wein Li[4], Lei Wan[1], Fuu-Jen Tsai[1] and Cheng-Wen Lin[4, 5]*

[1] Department of Medical Genetics and Medical Research, China Medical University Hospital, Taichung, Taiwan
[2] Institute of Molecular Biology, National Chung Hsing University, Taichung, Taiwan
[3] Department of Anatomy, School of Medicine, China Medical University, Taichung, Taiwan
[4] Department of Medical Laboratory Science and Biotechnology, China Medical University, Taichung, Taiwan
[5] Clinical Virology Laboratory, Department of Laboratory Medicine, China Medical University Hospital, Taichung, Taiwan

Received: June 23, 2006
Revised: November 29, 2006
Accepted: January 28, 2007

The pathogenesis of severe acute respiratory syndrome coronavirus (SARS CoV) is an important issue for treatment and prevention of SARS. Previously, SARS CoV 3C-like protease (3CLpro) has been demonstrated to induce apoptosis *via* the activation of caspase-3 and caspase-9 (Lin, C. W., Lin, K. H., Hsieh, T. H., Shiu, S. Y. *et al.*, *FEMS Immunol. Med. Microbiol.* 2006, *46*, 375–380). In this study, proteome analysis of the human promonocyte HL-CZ cells expressing SARS CoV 3CLpro was performed using 2-DE and nanoscale capillary LC/ESI quadrupole-TOF MS. Functional classification of identified up-regulated proteins indicated that protein metabolism and modification, particularly in the ubiquitin proteasome pathway, was the main biological process occurring in SARS CoV 3CLpro-expressing cells. Thirty-six percent of identified up-regulated proteins were located in the mitochondria, including apoptosis-inducing factor, ATP synthase beta chain and cytochrome c oxidase. Interestingly, heat shock cognate 71-kDa protein (HSP70), which antagonizes apoptosis-inducing factor was shown to down-regulate and had a 5.29-fold decrease. In addition, confocal image analysis has shown release of mitochondrial apoptogenic apoptosis-inducing factor and cytochrome c into the cytosol. Our results revealed that SARS CoV 3CLpro could be considered to induce mitochondrial-mediated apoptosis. The study provides system-level insights into the interaction of SARS CoV 3CLpro with host cells, which will be helpful in elucidating the molecular basis of SARS CoV pathogenesis.

Keywords:
2-DE / 3C-like protease / MS / Severe acute respiratory syndrome (SARS) coronavirus

Correspondence: Dr. Cheng-Wen Lin, Department of Medical Laboratory Science and Biotechnology, China Medical University, No. 91, Hsueh-Shih Road, Taichung 404, Taiwan
E-mail: cwlin@mail.cmu.edu.tw
Fax: +886-4-2205-7414

Abbreviations: 3CLpro, 3C-like protease; **Q-TOF**, quadrupole-time of flight; **SARS CoV**, severe acute respiratory syndrome coronavirus

1 Introduction

A novel virus, severe acute respiratory syndrome (SARS)-associated coronavirus (SARS CoV) is rapidly transmitted through aerosols, causing 8447 reported SARS cases with

* Additional corresponding author: Professor Fuu-Jen Tsai
E-mail: d0704@www.cmuh.org.tw

811 deaths worldwide in a short period from February to June, 2003 [1–5]. The SARS patients had manifested symptoms, like bronchial epithelial denudation, loss of cilia, multinucleated syncytial cells and squamous metaplasia in their lung tissue [6, 7]. Other studies have shown that SARS CoV replicates in Vero-E6 cells with cytopathic effects [8, 9], and induces AKT signaling-mediated cell apoptosis [10].

SARS CoV particles contain an approximately 30-kbp positive-stranded RNA genome with a 5' cap structure and a 3' poly(A) tract [11–13]. The SARS CoV genome encodes replicase, spike, envelope, membrane, and nucleocapsid proteins. The replicase gene encodes two large overlapping polypeptides (replicase 1a and 1ab, ~450 and ~750 kDa, respectively), including 3C-like protease (3CLpro), RNA-dependent RNA polymerase, and RNA helicase for viral replication and transcription [14]. The SARS CoV 3CLpro mediates the proteolytic processing of replicase 1a and 1ab into functional proteins, playing an important role in viral replication. Therefore, the SARS CoV 3CLpro is an attractive target for developing effective drugs against SARS [12–14]. Recently, a SARS CoV 3CLpro-interacting cellular protein, vacuolar-H+ ATPase (V-ATPase) G1 subunit with a 3CLpro cleavage site-like motif was identified, affecting the intracellular pH in 3CLpro-expressing cells [15]. In human promonocyte cells, SARS CoV 3CLpro has been demonstrated to induce apoptosis *via* caspase-3 and caspase-9 activities [16]. In addition, 3C protease of picornaviruses poliovirus, enterovirus 71 and rhinovirus have been demonstrated to be associated with host translation shutoff by cleaving the translation initiation factor eIF4GI and the poly(A)-binding protein (PABP) [17], and inactivation of NF-kappaB function by proteolytic cleavage of p65-RelA [18]. Apparently, SARS CoV 3CLpro plays a pivotal role in the pathogenesis processes. Therefore, investigating pathogenesis of SARS CoV 3CLpro has become an important issue.

In the post-genomic era, the combination of 2-DE and MS has provided an alternative approach to examine a comparative analysis of proteomic profiling during viral infection, allowing new insights into cellular mechanisms involved in viral pathogenesis [19–24]. The 2-DE/MS proteomic technologies have been used to analyze the protein profiles of plasma from SARS patients [19, 24], and to differentiate up-regulated and down-regulated proteins in SARS CoV-infected African green monkey kidney cells [20]. To identify proteomic alternations induced by SARS CoV 3CLpro, the combination of 2-DE and MS can be performed for quantitative analysis and identification of the unique protein profiling in the transfected cells-expressing 3CLpro.

In this study, we intended to investigate the comparative proteome analysis of human promonocyte HL-CZ cells in the presence and absence of SARS CoV 3CLpro. Seventy-three up-regulated and 21 down-regulated proteins identified in the 3CLpro-expressing cells were categorized according to their subcellular location, biological process and biological pathway based upon the PANTHER classification system (http://www.pantherdb.org/). Functional analysis of up-regulated proteins identified in the 3CLpro-expressing cells was further examined using immunoblot analysis and confocal microscopy.

2 Materials and methods

2.1 Cell culture

In our previous study [16], human promonocyte HL-CZ cell clone co-transfected with the plasmid p3CLpro plus indicator vector pEGFP-N1 was established for 3CLpro-expressing cells, whereas human promonocyte HL-CZ cell clones co-transfected with the plasmid pcDNA3.1 plus indicator vector pEGFP-N1 were used as mock cells. The transfected cells were incubated with RPMI 1640 medium containing 10% FBS and 800 μg/mL of antibiotic G418. For determining expression of SARS CoV 3CLpro, the transfected cells were analyzed using Western blotting. The cell lysates were dissolved in 2X SDS-PAGE sample buffer without 2-mercaptoethanol, and boiled for 10 min. Proteins were resolved on 12% SDS-PAGE gels and transferred to NC paper. The resultant blots were blocked with 5% skim milk, and then reacted with appropriately diluted mouse mAb anti-His tag (Serotec), anti-Rpt4 (26S protease regulatory subunit 6A) (abcam) or rabbit anti-apoptosis-inducing factor (Sigma) for a 3-h incubation. The blots were then washed with TBST three times and overlaid with a 1/5000 dilution of alkaline phosphatase-conjugated with secondary antibodies. Following 1-h incubation at room temperature, blots were developed with TNBT/BCIP (Gibco).

2.2 2-DE and protein spot analysis

For 2-DE, mock cells and 3CLpro-expressing cells were harvested, washed twice with ice-cold PBS, and then extracted with lysis buffer containing 8 M urea, 4% CHAPS, 2% pH 3–10 non-linear (NL) IPG buffer (GE Healthcare), and the Complete, Mini, EDTA-free protease inhibitor mixture (Roche). After a 3-h incubation at 4°C, the cell lysates were centrifuged for 15 min at 16 000 × *g*. The protein concentration of the resulting supernatants was measured using the BioRad Protein Assay (BioRad, Hercules, CA, USA). Protein sample (100 μg) was diluted with 350 μL of rehydration buffer (8 M urea, 2% CHAPS, 0.5% IPG buffer pH 3–10 NL, 18 mM DTT, 0.002% bromophenol blue), and then applied to the nonlinear Immobiline DryStrips (17 cm, pH 3–10; GE Healthcare). After the run of 1-D IEF on a Multiphor II system (GE Healthcare), the gel strips were incubated for 30 min in the equilibration solution I (6 M urea, 2% SDS, 30% glycerol, 1% DTT, 0.002% bromophenol blue, 50 mM Tris-HCl, pH 8.8), and for another 30 min in the equilibration solution II (6 M urea, 2% SDS, 30% glycerol, 2.5% iodoacetamide, 0.002% bromophenol blue, 50 mM Tris-HCl, pH 8.8). Subsequently, the IPG gels were transferred to the top of 12% polyacrylamide gels (20 × 20 cm × 1.0 mm) for

the secondary dimensional run at 15 mA, 300 V for 14 h. Separated protein spots were fixed in the fixing solution (40% ethanol and 10% glacial acetic acid) for 30 min, stained on the gel with silver nitrate solution for 20 min, and then scanned by GS-800 imaging densitometer with PDQuest software version 7.1.1 (BioRad). Data from three independently stained gels of each sample were exported to Microsoft Excel for creation of the correction graphs, spot intensity graphs and statistical analysis.

2.3 In-gel digestion

The modified in-gel digestion method based on previous reports [25, 26] was performed for nanoelectrospray MS. Briefly, each spot of interest in the silver-stained gel was sliced and put into the microtube, and then washed twice with 50% ACN in 100 mM ammonium bicarbonate buffer (pH 8.0) for 10 min at room temperature. Subsequently, the excised-gel pieces were soaked in 100% ACN for 5 min, dried in a lyophilizer for 30 min and rehydrated in 50 mM ammonium bicarbonate buffer (pH 8.0) containing 10 μg/mL trypsin at 30°C for 16 h. After digestion, the peptides were extracted from the supernatant of the gel elution solution (50% ACN in 5.0% TFA), and dried in a vacuum centrifuge.

2.4 Nanoelectrospray MS and database search

The proteins were identified using an Ultimate capillary LC system (LC Packings, Amsterdam, The Netherlands) coupled to a QSTARXL quadrupole-time of flight (Q-TOF) mass spectrometer (Applied Biosystem/MDS Sciex, Foster City, CA, USA). The peptides was separated using an RP C18 capillary column (15 cm × 75 μm id) with a flow rate of 200 nL/min, and eluted with a linear ACN gradient from 10–50% ACN in 0.1% formic acid for 60 min. The eluted peptides from the capillary column were sprayed into the MS by a PicoTip electrospray tip (FS360-20-10-D-20; New Objective, Cambridge, MA, USA). Data acquisition from Q-TOF was performed using the automatic Information Dependent Acquisition (IDA; Applied Biosystem/MDS Sciex). Proteins were identified by the nanoLC-MS/MS spectra by searching against NCBI databases for exact matches using the ProID program (Applied Biosystem/MDS Sciex) and the MASCOT search program (http://www.matrixscience.com) [27]. A Homo sapiens taxonomy restriction was used and the mass tolerance of both precursor ion and fragment ions was set to ± 0.3 Da. Carbamidomethyl cysteine was set as a fixed modification, while serine, threonine, tyrosine phosphorylation and other modifications were set as variable modifications. The protein function and subcellular location were annotated using the Swiss-Prot (http://us.expasy.org/sprot/). The proteins were also categorized according to their biological process and pathway using the PANTHER classification system (http://www.pantherdb.org) as described in the previous studies [28–30].

2.5 Immunocytochemistry

For determining subcellular localization, HL-CZ cells were transiently co-transfected with p3CLpro or pcDNA3.1 plus a mitochondrial localization vector pDsRed-Mito (Clontech) using the GenePorter reagent. After a 3-day incubation, the cells were fixed on glass coverslips with ice-cold acetone for 4 min, and blocked with 1% BSA. The co-transfected cells were subsequently incubated with mouse mAb anti-His tag, anti-cytochrome c, or rabbit anti-apoptosis-inducing factor (Sigma) at 4°C overnight. After washing, the cells were incubated with FITC–conjugated goat anti-mouse immunoglobulin or anti-rabbit immunoglobulin at room temperature for 2 h. Confocal image analysis of the cells was performed using Leica TCS SP2 AOBS laser-scanning microscopy (Leica Microsystems, Heidelberg, Germany).

3 Results

3.1 Comparison of differential protein expression between mock cells and SARS CoV 3CLpro-expressing cells

To identify specific cell responses to SARS CoV 3CLpro, the differential expression of proteins in mock cells and 3CLpro-expressing cells were analyzed using 2-DE and nanoscale capillary LC/ESI Q-TOF MS. After confirming expression of SARS CoV 3CLpro in the transfected cells as previously described [16], protein extracts prepared from mock cells and 3CLpro-expressing cells were separated using 2-DE. The resolved protein spots in gels were presented using silver staining (Fig. 1). About 1000 protein spots in the p*I* range of 3.2 to 10 and the molecular weight range of 14 to 97.4 kDa were detected on the gels of mock (Fig. 1A) and 3CLpro-expressing cells (Fig. 1B), respectively. For comparison, three independent 2-DE images of each protein extract from three independent cell cultures of mock cells and 3CLpro-expressing cells were selected for statistical analysis. Protein profiling revealed that 154 ± 15 up-regulated proteins and 141 ± 12 down-regulated proteins in SARS CoV 3CLpro-expressing cells were determined using GS-800 imaging densitometer with PDQuest software (Fig. 1). After the statistical analysis with Student's *t*-test, 75 up-regulated proteins (Spot ID number between 1 and 75) showed a statistically significant 1.5-fold increase in spot intensity ($p<0.05$) (Table 1), whereas 21 down-regulated proteins (Spot ID number between 76 and 96) had a statistically significant 2.0-fold decrease in 3CLpro-expressing cells (Table 2). Moreover, enlarged images of the selected protein spots were used to indicate spots with significant differences between mock cells and 3CLpro-expressing cells (Fig. 2). A dramatic (greater than 100-fold) increase for Spot ID 19, a 3.3 ± 0.13-fold increase for Spot ID 55, a 5.29 ± 0.12-fold decrease for Spot ID 83, and a 6.25 ± 0.09-fold decrease for Spot ID 89 were found in 3CLpro-expressing cells (Fig. 2, Tables 1 and

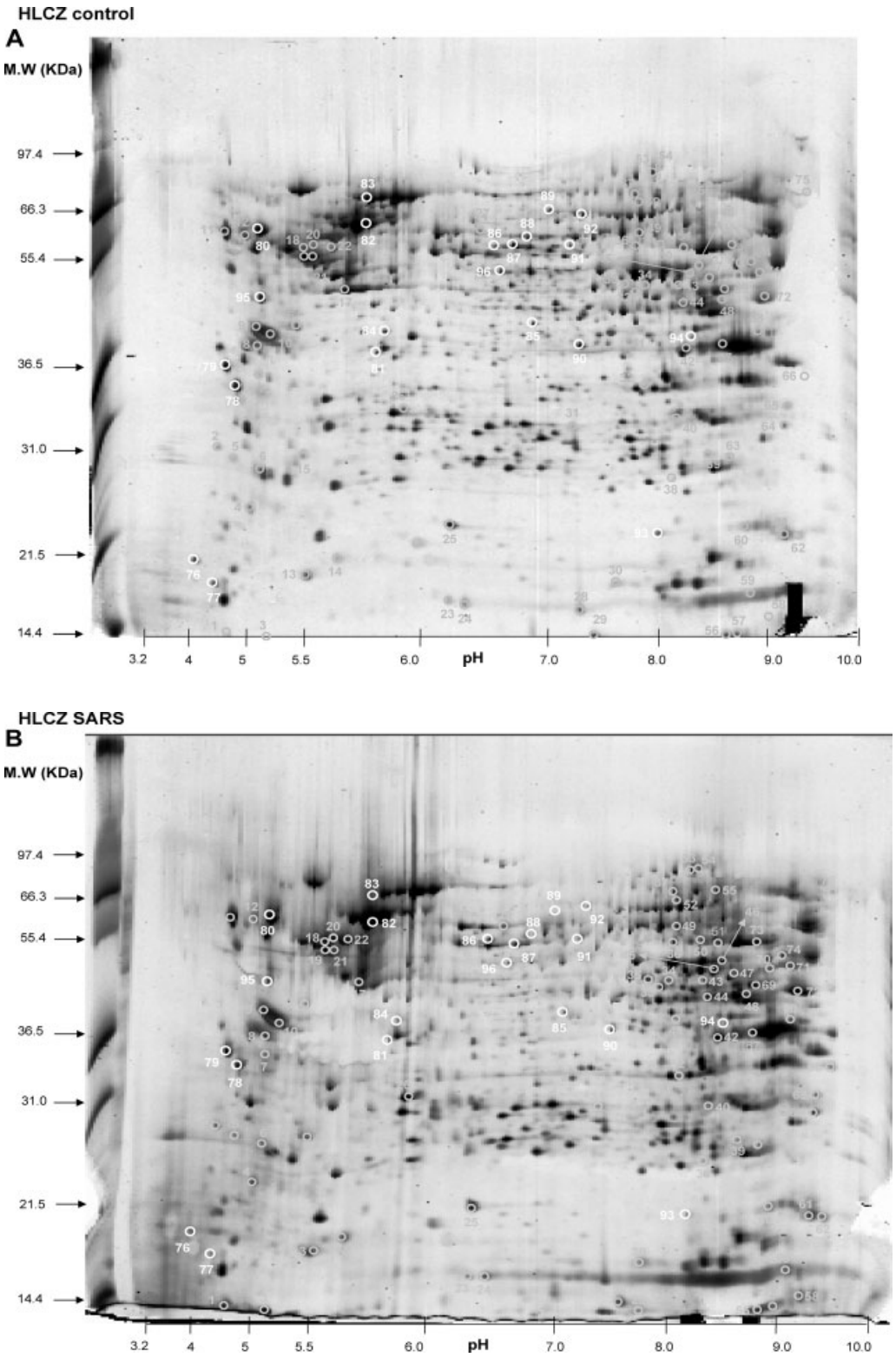

Figure 1. 2-DE image for total cell extracts from human promonocyte HL-CZ cells (A) and SARS CoV 3CLpro-expressing cells (B). Protein sample (100 μg) was diluted with 350 μL of rehydration buffer, and then applied to the nonlinear Immobiline DryStrip (17 cm, pH 3–10). After incubation in the equilibration solutions, the IPG gels were transferred to the top of 12% polyacrylamide gels (20 × 20 cm × 1.0 mm). Finally, the 2-DE gels were stained with the silver nitrate solution. Protein size markers are shown at the left of each gel (in kDa). The protein spot ID numbers were consistent with those in Tables 1 and 2.

Table 1. Identification and functional classification of up-regulated proteins in SARS CoV 3CLpro-expressing cells. Biological processes associated with up-regulated proteins were categorized using Panther classification system

Biological process	Spot ID	Accession No.	PANTHER Gene ID	Protein identification	Subcellular location	MW (KDa)/p*I*	Score	Peptide match	Sequence coverage (%)	Fold change Mean	SD	*p* value[a)]
Pre-mRNA processing												
	16	P07910	3183	Heterogeneous nuclear ribonucleoproteins C1/C2	Nucleus	33.7/5.0	362	8	22	>100		<0.001
	37	Q96AE4	8880	Far upstream element binding protein 1	Nucleus	67.4/7.2	478	15	22	1.9	0.10	0.002
	41	Q99729	3182	Heterogeneous nuclear ribonucleoprotein A/B	Nucleus	36.6/9.0	69	3	9	10.7	0.36	<0.001
	47	Q14103	3184	Heterogeneous nuclear ribonucleoprotein D0	Nucleus	38.4/7.6	216	4	12	3.6	0.08	<0.001
	53	Q92945	8570	Far upstream element binding protein 2	Nucleus	72.7/8.0	1082	31	44	2.5	0.07	0.001
	68	P22626	3181	Heterogeneous nuclear ribonucleoproteins A2/B1	Nucleus	37.4/9.0	607	17	36	3.5	0.09	<0.001
	70	Q96EP5	26528	DAZ-associated protein 1	Cytoplasm	43.4/8.7	124	3	9	2.7	0.05	0.001
	75	P52272	4670	Heterogeneous nuclear ribonucleoprotein M	Nucleus and nucleolar	77.3/8.9	725	17	27	5	0.14	<0.001
Electron transport												
	1	P07919	7388	Ubiquinol-cytochrome c reductase complex 11 kDa protein	Mitochondrion	10.7/4.4	88	3	36	5.6	0.14	<0.001
	4	O43169	80777	Cytochrome b5 outer mitochondrial membrane isoform	Mitochondrion	16.3/4.88	224	5	55	1.9	0.15	0.002
	19	P06576	506	ATP synthase beta chain	Mitochondrion	56.5/5.3	973	19	42	>100		<0.001
	29	P10606	1329	Cytochrome c oxidase polypeptide Vb	Mitochondrion	13.7/9.1	149	5	24	>100		<0.001
	33	P11310	34	Acyl-CoA dehydrogenase, medium-chain specific	Mitochondrion	46.6/8.6	652	16	45	3.8	0.09	<0.001
	46	P22570	2232	NADPH:adrenodoxin oxidoreductase	Mitochondrion	53.8/8.6	166	10	21	2.3	0.14	0.001
	49	P09622	1738	Dihydrolipoyl dehydrogenase		54.1/7.6	342	10	22	2.1	0.12	0.001
	50	P00390	2936	Glutathione reductase	Mitochondrion and cytoplasm	56.2/8.7	111	5	11	>100		<0.001
Protein metabolism and modification												
	8	O43765	6449	Small glutamine-rich tetratricopeptide repeat-containing protein A		34.0/4.8	185	6	18	>100		<0.001
	11	P27797	811	Calreticulin	Endoplasmic reticulum	48.1/4.3	988	54	70	>100		<0.001
	13	P63241	1984	Eukaryotic translation initiation factor 5A		16.7/5.1	29	2	13	>100		<0.001
	18	Q15084	10130	Protein disulfide-isomerase A6	Endoplasmic reticulum	48.1/4.95	389	5	15	>100		<0.001
	20	Q8NBS9	81567	Thioredoxin domain-containing protein 5	Endoplasmic reticulum	47.6/5.3	259	7	16	>100		<0.001
	21	P17980	5702	26S protease regulatory subunit 6A	Cytoplasm and nucleus	49.2/5.1	107	4	11	2.8	0.09	<0.001
	23	Q99471	5204	Prefoldin subunit 5		17.3/5.9	82	1	11	11.0	0.24	<0.001
	24	P61088	7334	Ubiquitin-conjugating enzyme E2 N		17.1/6.1	217	8	52	6.5	0.11	<0.001
	27	P30101	2923	Protein disulfide-isomerase A3	Endoplasmic reticulum	56.8/6.0	436	12	23	5.9	0.17	<0.001
	28	P25398	6206	40S ribosomal protein S12	Cytoplasm	14.4/6.4	266	8	51	>100		<0.001
	30	P62937	5478	Peptidyl-prolyl cis-trans isomerase A	Cytoplasm	17.9/7.8	312	7	40	1.8	0.14	0.003
	35	P49411	7284	Elongation factor Tu	Mitochondrion	49.5/7.3	280	7	21	4.3	0.12	<0.001
	37	Q96AE4	8880	Far upstream element binding protein 1	Nuclear	67.4/7.2	478	15	22	1.9	0.10	0.002
	39	P20618	5689	Proteasome subunit beta type 1	Cytoplasm and nucleus	26.5/8.3	125	4	19	2.4	0.14	0.001
	48	P24752	38	Acetyl-CoA acetyltransferase	Mitochondrion	45.1/9.0	392	9	29	3.1	0.27	<0.001
	53	Q92945	8570	Far upstream element binding protein 2	Nuclear	72.7/8.0	1082	31	44	2.5	0.07	0.001
	57	P52758	10247	Ribonuclease UK114	Cytoplasm	14.5/8.7	82	3	31	>100		<0.001
	61	P23284	5479	Peptidyl-prolyl cis-trans isomerase B	Endoplasmic reticulum	22.7/9.3	100	3	14	2.4	0.05	0.001
	65	Q00688	2287	FK506-binding protein 3	Nucleus	25.2/9.3	233	7	31	4.9	0.11	<0.001

Table 1. Continued

Biological process	Spot ID	Accession No.	PANTHER Gene ID	Protein identification	Subcellular location	MW (KDa)/p*I*	Score	Peptide match	Sequence coverage (%)	Fold change Mean	SD	*p* value[a)]
	71	P50454	871	Collagen-binding protein 2 precursor	Endoplasmic reticulum	46.4/8.8	259	7	21	>100		<0.001
Nucleoside, nucleotide and nucleic acid metabolism												
	6	P83916	10951	Chromobox protein homolog 1		21.4/4.9	316	5	30	>100		<0.001
	9	P51858	3068	Hepatoma-derived growth factor	Cytoplasm	26.8/4.7	372	11	48	5.1	0.13	<0.001
	10	P06748	4869	Nucleophosmin	Nucleus	32.6/4.6	865	36	72	2.7	0.19	0.001
	16	P07910	3183	Heterogeneous nuclear ribonucleoproteins C1/C2	Nucleus	33.7/5.0	362	8	22	>100		<0.001
	19	P06576	506	ATP synthase beta chain	Mitochondrion	56.5/5.3	973	19	42	>100		<0.001
	25	P15531	4830	Nucleoside diphosphate kinase A	Nucleus and cytoplasm	17.1/5.8	203	9	44	>100		<0.001
	26	P35232	5245	Prohibitin	Mitochondrion	29.8/5.6	831	20	75	>100		<0.001
	37	Q96AE4	8880	Far upstream element binding protein 1	Nucleus	67.4/7.2	478	15	22	1.9	0.10	0.002
	40	P54819	204	Adenylate kinase isoenzyme 2	Mitochondrion	26.3/7.9	177	4	21	4.7	0.13	<0.001
	41	Q99729	3182	Heterogeneous nuclear ribonucleoprotein A/B	Nucleus	36.6/9.0	69	3	9	10.7	0.36	<0.001
	47	Q14103	3184	Heterogeneous nuclear ribonucleoprotein D0	Nucleus	38.4/7.6	216	4	12	3.6	0.08	<0.001
	51	P34897	6472	Serine hydroxymethyltransferase	Mitochondrion	56.0/8.8	661	17	35	2.8	0.10	<0.001
	53	Q92945	8570	Far upstream element binding protein 2	Nucleus	72.7/8.0	1082	31	44	2.5	0.07	0.001
	62	O00422	10284	Histone deacetylase complex subunit SAP18		17.6/9.4	260	9	52	>100		<0.001
	64	Q9UIJ7	50808	GTP:AMP phosphotransferase mitochondrial	Mitochondrion	25.4/9.2	595	15	65	2.8	0.15	<0.001
	65	Q00688	2287	FK506-binding protein 3	Nucleus	25.2/9.3	233	7	31	4.9	0.11	<0.001
	68	P22626	3181	Heterogeneous nuclear ribonucleoproteins A2/B1	Nucleus	37.4/9.0	607	17	36	3.5	0.09	<0.001
	70	Q96EP5	26528	DAZ-associated protein 1	Cytoplasm	43.4/8.7	124	3	9	2.7	0.05	0.001
	75	P52272	4670	Heterogeneous nuclear ribonucleoprotein M	Nucleus and nucleolar	77.3/8.9	725	17	27	5	0.14	<0.001
Carbohydrate metabolism												
	31	P30084	1892	Enoyl-CoA hydratase	Mitochondrion	31.4/8.3	98	2	11	4.7	0.13	<0.001
	34	P08559	5160	Pyruvate dehydrogenase E1 component alpha subunit	Mitochondrion	43.3/8.4	121	2	5	>100		<0.001
	52	Q16822	5106	Phosphoenolpyruvate carboxykinase	Mitochondrion	70.6/7.6	917	20	35	>100		<0.001
	54	Q99798	50	Aconitate hydratase	Mitochondrion	85.4/7.4	820	25	40	>100		<0.001
	67	P40926	4191	Malate dehydrogenase	Mitochondrion	35.5/8.9	339	8	28	2.1	0.13	0.001
	69	P00558	5230	Phosphoglycerate kinase 1	Cytoplasm	44.5/8.3	441	11	30	>100		<0.001
Cell structure												
	7	P06753	7170	Tropomyosin alpha 3 chain		32.8/4.7	156	5	14	2.2	0.10	0.001
	17	P63261	71	Actin, cytoplasmic 2	Cytoplasm	41.8/5.3	263	11	32	69.6	2.16	<0.001
	22	P08670	7431	Vimentin		53.8/5.1	2401	84	85	>100		<0.001
Immunity and defense												
	30	P62937	5478	Peptidyl-prolyl cis-trans isomerase A	Cytoplasm	17.9/7.8	312	7	40	1.8	0.14	0.003
	38	P04179	6648	Superoxide dismutase [Mn]	Mitochondrion	24.7/8.4	87	2	9	2.3	0.09	0.001

Table 1. Continued

Biological process	Spot ID	Accession No.	PANTHER Gene ID	Protein identification	Subcellular location	MW (KDa)/p*I*	Score	Peptide match	Sequence coverage (%)	Fold change Mean SD	*p* value[a)]
	61	P23284	5479	Peptidyl-prolyl cis-trans isomerase B	Endoplasmic reticulum	22.7/9.3	100	3	14	2.4	0.05	0.001
	65	Q00688	2287	FK506-binding protein 3	Nucleus	25.2/9.3	233	7	31	4.9	0.11	<0.001
Cell cycle												
	17	P63261	71	Actin, cytoplasmic 2	Cytoplasm	41.8/5.3	263	11	32	69.6	2.16	<0.001
	26	P35232	5245	Prohibitin	Mitochondrion	29.8/5.6	831	20	75	>100		<0.001
	65	Q00688	2287	FK506-binding protein 3	Nucleus	25.2/9.3	233	7	31	4.9	0.11	<0.001
Amino acid biosynthesis												
	42	P13995	10797	methylenetetrahydrofolate dehydrogenase/cyclohydrolase	Mitochondrion	37.3/8.9	173	4	16	2.4	0.15	0.001
	44	Q9Y617	29968	Phosphoserine aminotransferase		40.4/7.6	394	10	29	>100		<0.001
Amino acid metabolism												
	45	P07954	2271	Fumarate hydratase	Mitochondrion and cytoplasm	54.6/8.9	373	9	24	2.8	0.06	<0.001
	72	P00505	2806	Aspartate aminotransferase	Mitochondrion	47.4/9.1	506	17	38	8	0.23	<0.001
Apoptosis												
	55	O95831	9131	Apoptosis-inducing factor	Mitochondrion	66.9/9.0	252	8	18	3.3	0.13	<0.001
Sulfur redox metabolism												
	5	O00264	10857	Membrane associated progesterone receptor component 1	Microsome	21.5/4.6	172	5	20	3.8	0.18	<0.001
Anion transport												
	66	P21796	7416	Voltage-dependent anion-selective channel protein 1	Mitochondrion	30.6/8.6	255	5	25	>100		<0.001
Steroid hormone-mediated signaling												
	14	O95881	51060	Thioredoxin domain-containing protein 12	Endoplasmic reticulum	19.2/5.2	191	6	57	12.7	0.14	<0.001
Muscle contraction												
	15	P12829	4635	Myosin light polypeptide 4		21.4/5.0	411	10	46	3.4	0.09	<0.001
Unclassified												
	2	Q9UMS0	27247	HIRA-interacting protein 5	Mitochondrion	21.8/4.2	286	6	33	2.1	0.16	
	3	P20674	9377	Cytochrome C oxidase polypeptide Va	Mitochondrion	16.8/6.3	267	8	46	>100		<0.001
	32	P13804	2108	Electron transfer flavoprotein alpha-subunit	Mitochondrion	35.1/8.6	763	15	56	1.6	0.21	0.005
	56	P07737	5216	Profilin-1		14.9/8.5	355	10	81	65.8	1.68	<0.001
	58	Q9NPJ3	55856	Thioesterase superfamily member 2		15.0/9.2	87	2	17	>100		<0.001
	59	P62807	8339	Histone H2B.a/g/h/k/l	Nucleus	13.8/10.3	211	6	40	>100		<0.001
	63	Q9Y2Q3	373156	Glutathione S-transferase kappa 1	Peroxisome	25.3/8.5	189	3	20	5.9	0.24	<0.001
	73	P25705	498	ATP synthase alpha chain	Mitochondrion	59.7/9.2	784	14	34	>100		<0.001

a) Student's *t*-test.

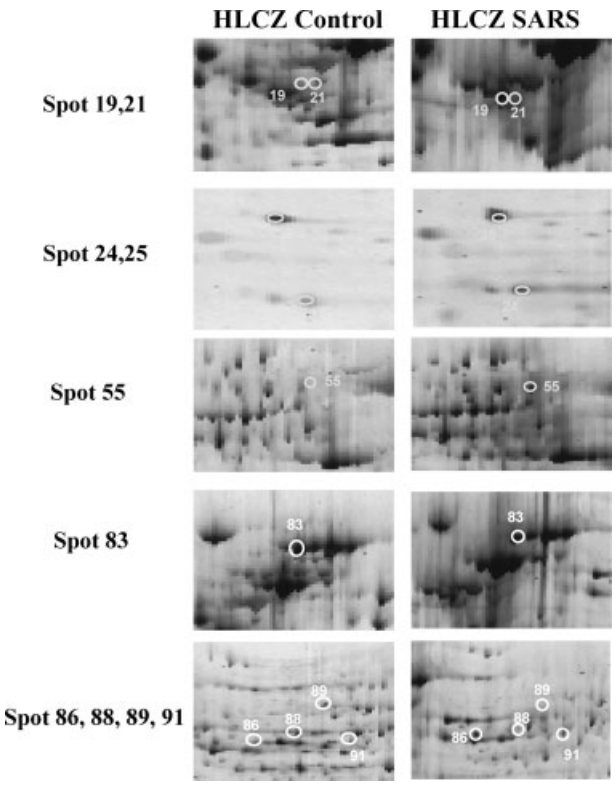

Figure 2. Close-up comparisons of spots on 2-DE images. The interested protein spots showing significant expression differences were enlarged. The circles indicated protein spots of total cell extracts from mock cells (left) and 3CLpro-expressing cells (right). The protein spot ID numbers were consistent with those in Tables 1 and 2.

2). These selected protein spots were picked out of the stained gel, subjected to in-gel tryptic digestion, and underwent PMF using the NanoLC Trap Q-TOF MS (Tables 1 and 2). The representative peptide peaks from Q-TOF MS analysis were detected, such as 26S protease regulatory subunit 6A (Spot ID 21) (Fig. 3A) and apoptosis-inducing factor (Spot ID 55) (Fig. 3B), resulting in confident protein identification by MASCOT searching. The search results indicated that 73 up-regulated and 21 down-regulated proteins showed the best match with a protein score of greater than or equal to 67, considered to be significant using the MASCOT search algorithm ($p<0.05$) (Tables 1 and 2). The amino acid sequence coverage of identified up-regulatory and down-regulatory proteins varied from 9 to 85%. For example, ubiquitin-conjugating enzyme E2 N (Spot ID 24) had a MASCOT score of 217, sequence coverage of 52%, and eight matched peptides, while apoptosis-inducing factor (Spot ID 55) showed a MASCOT score of 252, sequence coverage of 18%, and eight matched peptides. Therefore, comparative analysis of protein profiling indicated that 73 up-regulated and 21 down-regulated proteins were identified in 3CLpro-expressing cells.

3.2 Functional classification of the identified up-regulated and down-regulated proteins

As for the implication of cellular responses to SARS CoV 3CLpro, these up-regulated and down-regulated proteins were further categorized according to their subcellular location, biological process and biological pathway using the PANTHER classification system (Figs. 4 and 5, Tables 1, 2 and 3). Interestingly, up-regulated proteins in 3CLpro-expressing cells were mainly located in the mitochondrion (26/73, 36%) (Fig. 4A). By contrast, down-regulated proteins were distributed within different parts of the cells (19% in mitochondrion, 24% in cytoplasm, and 10% in nucleus) (Fig. 4B). Biological process categorization revealed a diversity of biological processes associated with the proteins identified (Fig. 5). The up-regulated proteins were responsible for the five main biological processes of protein metabolism and modification, nucleoside, nucleotide and nucleic acid metabolism, electron transport, pre-mRNA processing, and immunity and defense (Fig. 5, Table 1). Comparison of the sub-categories of protein metabolism and modification showed significant differences between the biological process of up-regulated and down-regulated proteins (Fig. 5). The biological processes of proteolysis and protein modification were significantly up-regulated, but the biological processes of the protein biosynthesis and protein complex assembly were down-regulated in 3CLpro-expressing cells. Furthermore, 26S protease regulatory subunit 6A (Spot ID 21) and ubiquitin-conjugating enzyme E2 N (Spot ID 24), which is up-regulated in the biological processes of proteolysis and protein modification that are key to the ubiquitin proteasome pathway (Table 3). According to the biological pathway categorization, up-regulated proteins are associated with 11 signaling pathways, including *de novo* purine biosynthesis, ubiquitin proteasome, ATP synthesis, and apoptosis signaling pathways (Table 3). Identified down-regulatory proteins in 3CLpro-expressing cells were involved in five signaling pathways, including *de novo* purine biosynthesis, apoptosis signaling, and mRNA splicing pathways (Table 3). Interestingly, analysis of apoptosis signaling pathway revealed that the mitochondrial apoptogenic apoptosis-inducing factor (Spot ID 55) was up-regulated and anti-apoptogenic heat shock cognate 71-kDa protein (HSP70) (Spot ID 83) was down-regulated in 3CLpro-expressing cells (Table 3). This finding suggested that expression of SARS CoV 3CLpro resulted in activation of the apoptosis signaling pathway.

3.3 Expression increases of 26S protease regulatory subunit 6A and apoptosis-inducing factor

To confirm the expression levels of these identified proteins, Western blotting analysis of cell lysates from mock cells and SARS-CoV 3CLpro-expressing cells was carried out, in which beta-actin was used as an internal control (Fig. 6). After normalization with beta-actin, densitometric analysis of immuno-

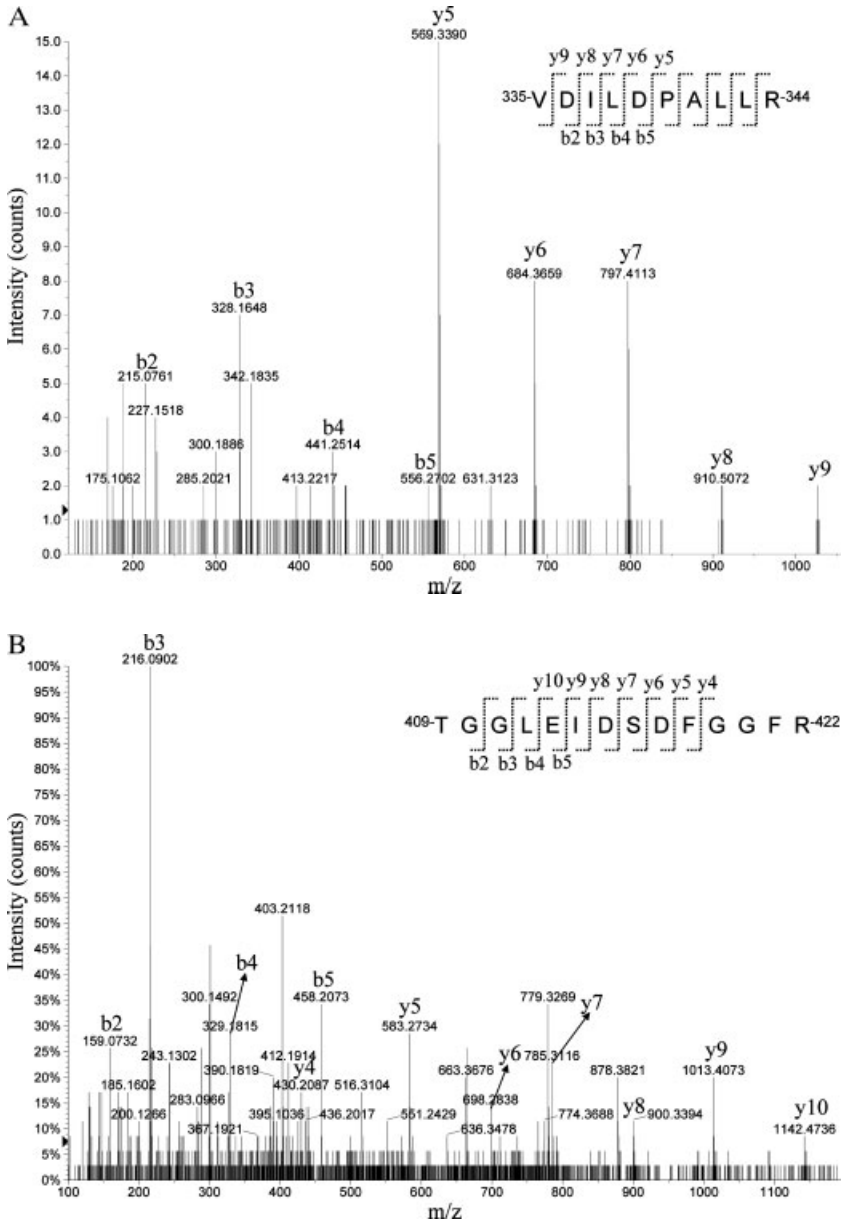

Figure 3. Identification of 26S protease regulatory subunit 6A (Spot ID 21) (A) and apoptosis-inducing factor (Spot ID 55) (B). (A) The nanoelectrospray mass spectrum of the doubly charged ion *m/z* 562.84 for Spot ID 21 is shown. The amino acid sequence VDILDPALLR was determined from mass differences in the y and b-fragment ions series and matched residues 335–344 of 26S protease regulatory subunit 6A. (B) The nanoelectrospray mass spectrum of the doubly charged ion *m/z* 735.88 for Spot ID 55 is shown. The amino acid sequence TGGLEIDSDFGGFR was determined from mass differences in the y and b-fragment ions series and matched residues 409–422 of apoptosis-inducing factor.

reactive bands revealed that 26S protease regulatory subunit 6A and apoptosis-inducing factor were significantly increased 3- and 1.5-fold, respectively, in 3CLpro-expressing cells. The results were consistent with proteomic analyses of silver-stained 2-DE gels as shown in Fig. 1.

3.4 Subcellular localization of apoptosis-inducing factor and cytochrome c

To further investigate the role of mitochondria in SARS 3CLpro-induced apoptosis, confocal imaging analysis was applied to determine subcellular localization of apoptosis-inducing factor (Fig. 7). HL-CZ cells were transiently co-transfected with pcDNA3.1 or p3CLpro plus a mitochondrial localization vector pDsRed-Mito. After immunofluorescent staining, apoptosis-inducing factor labeled with FITC-conjugated secondary antibodies showed green fluoresce, whereas mitochondria were targeted by red fluorescent proteins (Fig. 7A). Confocal imaging of the stained cells revealed that the release of apoptosis-inducing factor from mitochondria was found in the SARS CoV 3CLpro-expressing cells (Fig. 7A, right), but not in mock cells (Fig. 7A, left). In addition, cytochrome c, the other mitochondrial pro-apoptotic protein, was also found to be released from mitochondria to cytosol in 3CLpro-expressing cells (Fig. 7B). The results indicated that SARS CoV 3CLpro induced mitochondria

Table 2. Identification and functional classification of down-regulated proteins in SARS CoV 3CLpro-expressing cells. Biological processes associated with down-regulated proteins were classified using Panther Classification system

Biological process	Spot ID	Accession No.	PANTHER Gene ID	Protein identification	Subcellular location	MW (KDa)/p*I*	Score	Peptide match	Sequence coverage (%)	Fold change Mean	SD	*p* value[a]
Protein metabolism and modification												
	76	P05386	6176	60S acidic ribosomal protein P1		11.5/4.26	152	2	51	2.89	0.09	<0.001
	77	P05387	6181	60S acidic ribosomal protein P2		11.7/4.42	385	7	77	4.27	0.13	<0.001
	78	P24534	1933	Elongation factor 1-beta		24.6/4.5	367	10	37	2.45	0.25	0.007
	80	P07237	5034	Protein disulfide-isomerase precursor	Endoplasmic reticulum	57.1/4.76	1097	30	51	5.73	0.31	<0.001
	82	P10809	3329	60 kDa heat shock protein	Mitochondrion	61.0/5.7	1404	39	43	2.27	0.19	0.005
	83	P11142	3312	Heat shock cognate 71 kDa protein	Cytoplasm	70.8/5.37	1287	31	47	5.29	0.12	<0.001
	84	Q13347	8668	Eukaryotic translation initiation factor 3 subunit 2		36.5/5.38	334	6	19	3.89	0.39	<0.001
	87	P78371	10576	T-complex protein 1 subunit beta	Cytoplasm	57.3/6.02	1566	34	58	7.35	0.13	<0.001
	92	P31948	10963	Stress-induced-phosphoprotein 1	Cytoplasm and nucleus	62.6/6.4	1091	30	46	4.1	0.09	<0.001
	96	Q9UQ80	5036	Proliferation-associated protein 2G4	Cytoplasm and nucleus	43.8/6.13	256	7	16	3.4	0.28	<0.001
Nucleoside, nucleotide and nucleic acid metabolism												
	88	Q9UMS4	27339	Pre-mRNA-splicing factor 19	Nucleus	55.1/6.14	357	10	22	3.24	0.11	<0.001
	89	P31939	471	Bifunctional purine biosynthesis protein PURH		64.6/6.27	397	10	19	6.25	0.09	<0.001
	93	P20290	689	Transcription factor BTF3	Nucleus	22.1/9.41	317	7	53	2.54	0.19	0.002
Cell structure and motility												
	81	P52907	829	F-actin capping protein alpha-1 subunit		32.9/5.45	486	11	53	3.52	0.28	<0.001
	90	P04083	301	Annexin A1		38.6/6.64	1299	22	63	7.03	0.15	<0.001
Immunity and defense												
	79	Q07021	708	Complement component 1, Q subcomponent-binding protein	Mitochondrion	31.3/4.74	321	5	21	8.59	0.3	<0.001
	83	P11142	3312	Heat shock cognate 71 kDa protein	Cytoplasm	70.8/5.37	1287	31	47	5.29	0.12	<0.001
Fatty acid biosynthesis												
	94	Q04828	1645	Aldo-keto reductase family 1 member C1	Cytoplasm	36.8/8.02	137	7	25	2.15	0.12	0.007
Other carbon metabolism												
	86	P05091	217	Aldehyde dehydrogenase	Mitochondrion	56.3/6.63	110	4	6	3.13	0.06	<0.001
	91	P00352	216	Retinal dehydrogenase 1	Cytoplasm	54.7/6.29	436	11	24	2.71	0.16	0.002
Unclassified												
	85	P82650	56945	Mitochondrial 28S ribosomal protein S22	Mitochondrion	41.2/7.7	466	14	31	3.54	0.2	<0.001
	95	P08865	3921	40S ribosomal protein SA (p40) (34/67 kDa laminin receptor)	Cytoplasm	32.7/4.79	512	12	43	6.65	0.31	<0.001

a) Student's *t*-test.

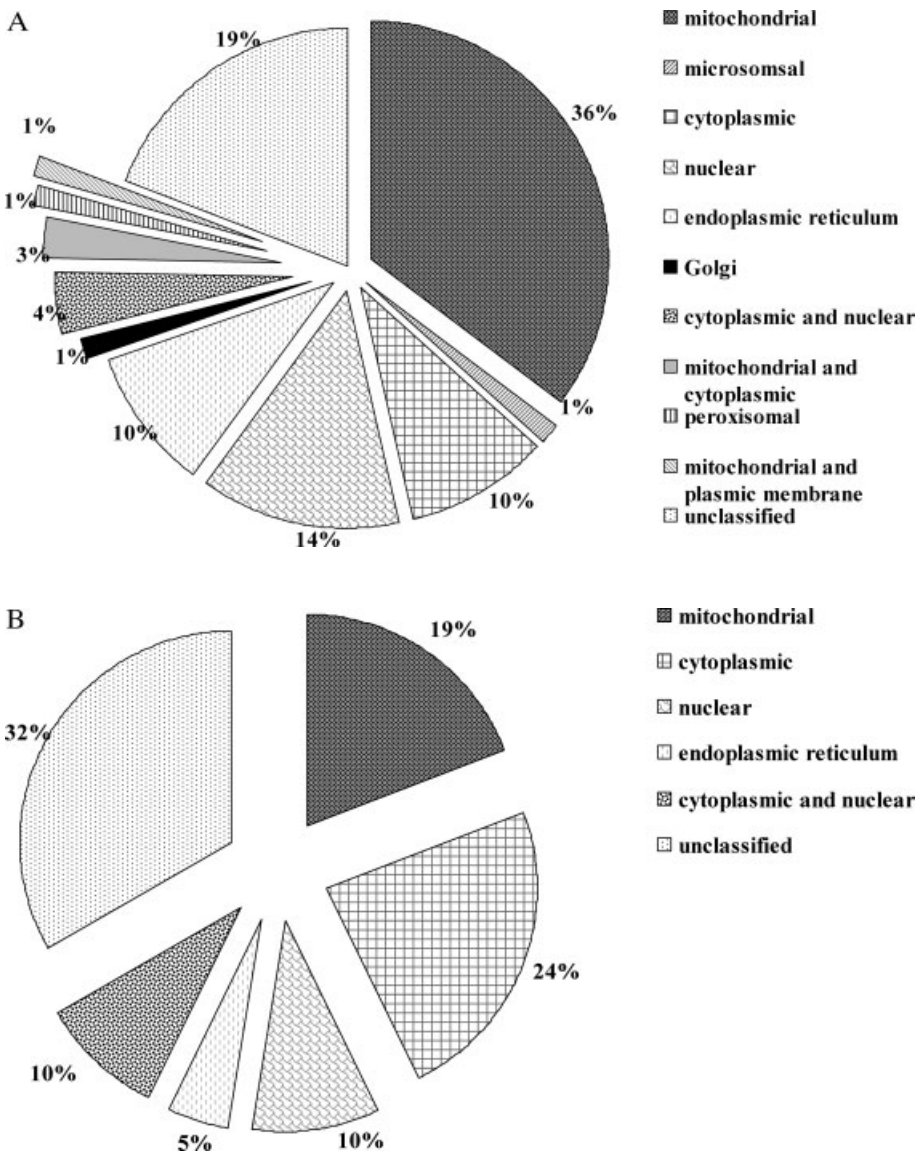

Figure 4. Subcellular localization of up-regulated (A) and down-regulated (B) proteins identified in 3CLpro-expressing cells. Subcellular localization of the identified proteins was classified using the Swiss-Prot.

alternations in release of apoptosis-inducing factor and cytochrome c, therefore responsible for activation of upstream caspase-9 and downstream caspase-3.

4 Discussion

In this study, 73 up-regulated and 21 down-regulated proteins in 3CLpro-expressing cells were identified using the combined analysis of 2-DE and Q-TOF MS (Figs. 1 and 2, Tables 1 and 2). Of the up-regulated proteins identified, 36% (26/73) were mitochondrial proteins that are associated with many biological processes, particularly in electron transport, ATP synthesis, carbohydrate metabolism and apoptosis (Fig. 4A, Table 1). By contrast, only 19% of down-regulated proteins were located within mitochondrion (Fig. 4B). Up-regulation of activation of the mitochondrial electron transport system coupled with ATP synthesis was identified in SARS 3CLpro-expressing cells (Fig. 5, Tables 1 and 3), in which ATP synthase (Spot ID 19) and cytochrome c oxidase were also in involved in the control of mitochondrial membrane potential $\Delta\Psi m$ and formation of reactive oxygen species (ROS) [31]. This finding could be associated with generation of ROS in 3CLpro-expressing cells as described in our previous report [16].

Protein metabolism and modification was the major biological process for up-regulated and down-regulated proteins in 3CLpro-expressing cells (Fig. 5). However, analysis of the biological process indicated that proteolysis and protein modification were significantly up-regulated, but protein biosynthesis and protein complex assembly were down-regulated in 3CLpro-expressing cells. Significant increases of

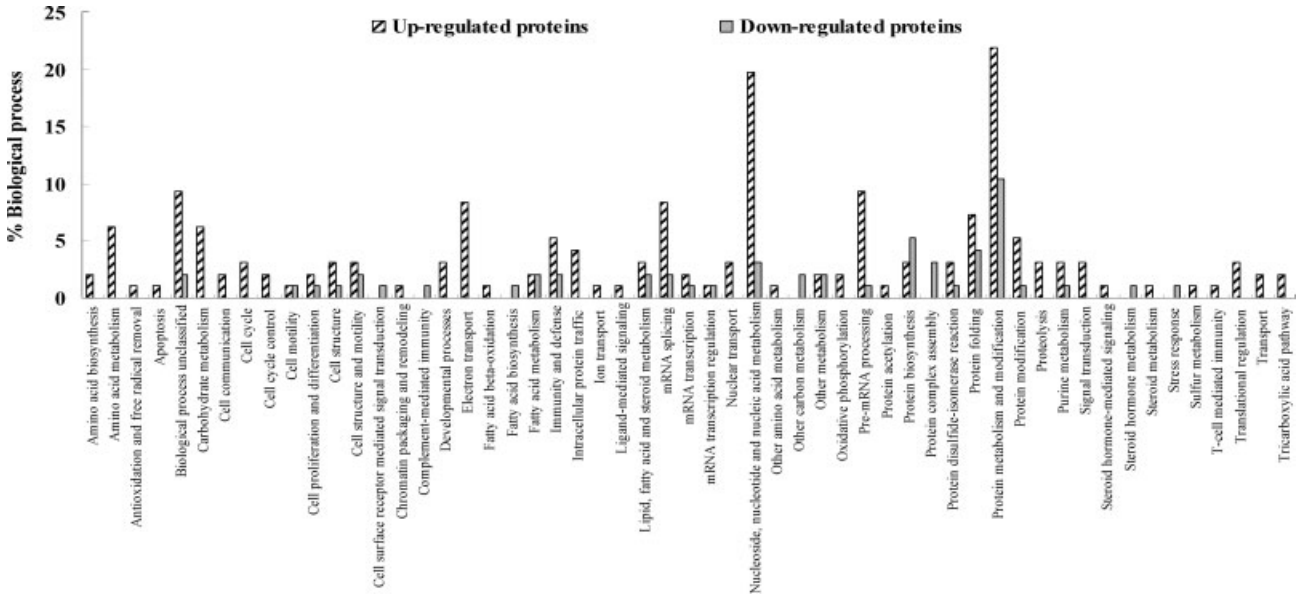

Figure 5. Comparison of biological processes associated with up-regulated and down-regulated proteins in 3CLpro-expressing cells compared with mock cells. Biological bioprocesses associated with up- and down-regulated proteins were classified using Panther Classification system (http://www.pantherdb.org/). Percent of biological process was calculated as the number of identified proteins in the indicated biological process/the number of the total identified proteins × 100.

Table 3. Comparison of biological pathways associated with up-regulated and down-regulated proteins in 3CLpro-expressing cells. Biological pathways associated with proteins identified were classified using Panther Classification system

Up-regulated proteins		Down-regulated proteins	
Pathways Spot ID	Protein identification	Pathways Spot ID	Protein identification
De novo purine biosynthesis		*De novo* purine biosynthesis	
25	Nucleoside diphosphate kinase A	89	Bifunctional purine biosynthesis protein PURH
40	Adenylate kinase isoenzyme 2		
64	GTP:AMP phosphotransferase mitochondrial		
Apoptosis signaling		Apoptosis signaling	
55	Apoptosis-inducing factor	83	Heat shock cognate 71 kDa protein
Ubiquitin proteasome		Phenylethylamine degradation	
21	26S protease regulatory subunit 6A	86	Aldehyde dehydrogenase
24	Ubiquitin-conjugating enzyme E2 N	91	Retinal dehydrogenase 1
ATP synthesis		mRNA splicing	
19	ATP synthase beta chain	88	Pre-mRNA-splicing factor 19
Glutamine glutamate conversion		5-Hydroxyptamine degradation	
36	Glutamate dehydrogenase 1	86	Aldehyde dehydrogenase
		91	Retinal dehydrogenase 1
Asparagine and aspartate biosynthesis			
72	Aspartate aminotransferase		
TCA cycle			
45	Fumarate hydratase		
Glycolysis			
69	Phosphoglycerate kinase 1		
62	Histone deacetylase complex subunit SAP18		
Toll receptor signaling pathway			
24	Ubiquitin-conjugating enzyme E2 N		
Cytoskeletal regulation by Rho GTPase			
56	Profilin-1		

the 26S protease regulatory subunit 6A (Spot ID 21) and ubiquitin-conjugating enzyme E2 N (Spot ID 24), which is involved in the ubiquitin proteasome pathway was demonstrated by sliver staining of 2-DE gels and Western blotting (Figs. 1, 2 and 6). Interestingly, up-regulation of proteasome subunits was also found in SARS CoV-infected Vero E6 cells and hepatitis virus B (HBV) HBx-expressing mice [20, 22]. The ubiquitin-proteasome pathway plays a central role in several cellular processes including antigen processing, apoptosis, cell cycle, inflammation, and response to stress [32], and is involved in the replication of several viruses, such as mouse hepatitis virus (murine coronavirus) [33, 34], adenovirus [35], hepatitis C virus [36], and human immunodeficiency virus [37]. Therefore, up-regulation of the ubiquitin-proteasome pathway induced by SARS-CoV 3CLpro protein might be involved in the SARS pathogenesis.

Five kinds (C1/C2, A/B, D0, A2/B1 and M) of heterogeneous nuclear ribonucleoproteins (hnRNP) were identified as being significantly up-regulated in SARS-CoV 3CLpro-expressing cells (Fig. 1, Table 1), and responsible for transcription, pre-mRNA processing, mRNA splicing, and nucleoside, nucleotide and nucleic acid metabolism (Fig. 5 and Table 1). The finding was in agreement with the protein profiling of SARS-CoV-infected cells in a previous report [20]. HnRNP have also been reported to be involved in the replication of mouse hepatitis virus (MHV) [38, 39]. In addition, hnRNP A2/B1 and A/B have been demonstrated to interact with the negative-strand MHV leader RNA and to enhance

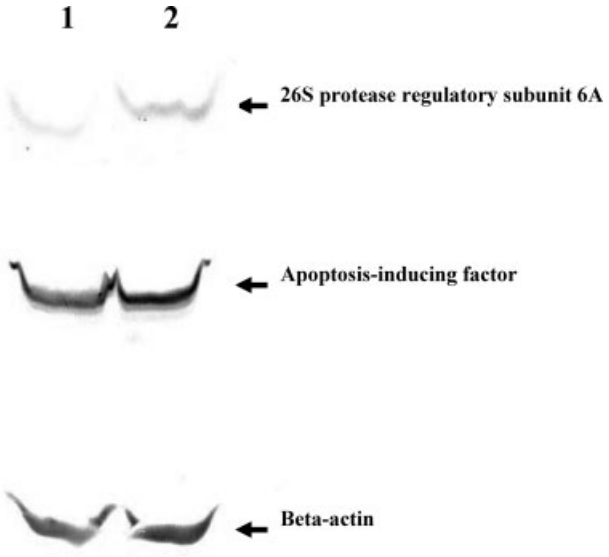

Figure 6. Western blot analysis of 26S protease regulatory subunit 6A and apoptosis-inducing factor in mock cells and 3CLpro-expressing cells. Each lysate was analyzed by 12% SDS-PAGE, and then electrophorectically transferred onto NC paper. The blot was probed with monoclonal antibodies to 26S protease regulatory subunit 6A and apoptosis-inducing factor, and developed with an alkaline phosphatase-conjugated secondary antibody and NBT/BCIP substrates. Lane 1: mock cells; lanes 2: 3CLpro-expressing cells.

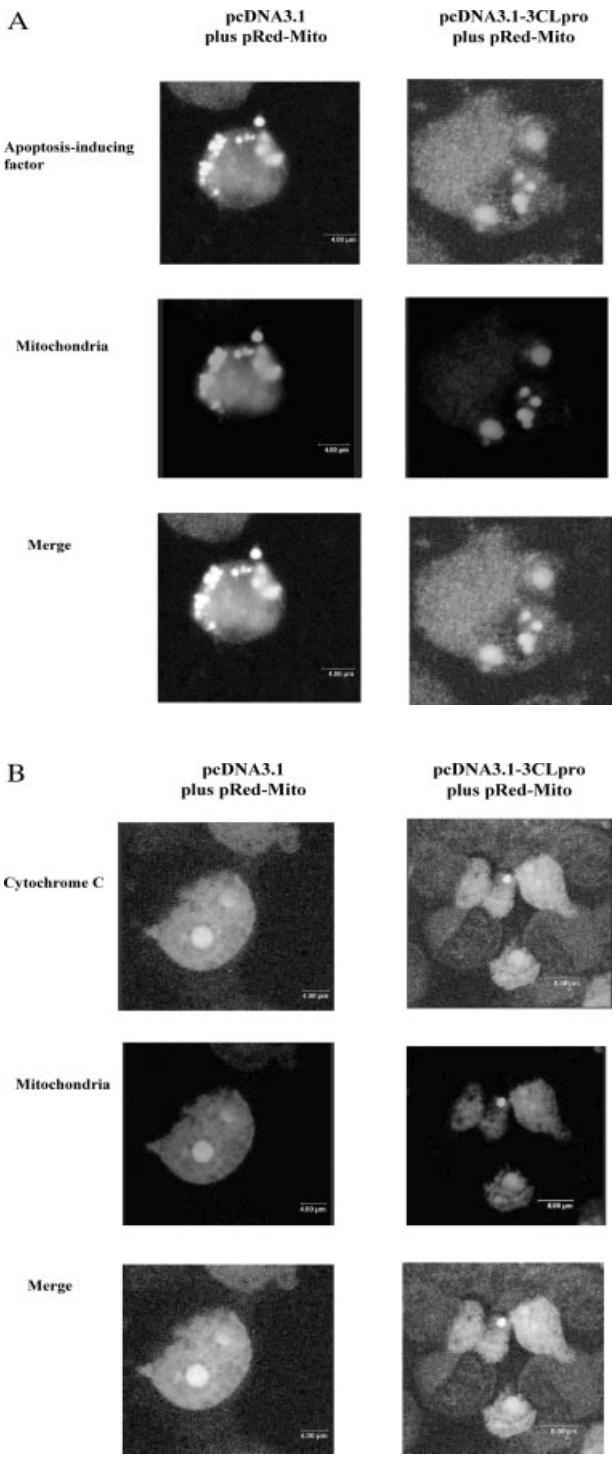

Figure 7. Confocal image analysis of apoptosis-inducing factor (A) and cytochrome c (B) in mock cells and 3CLpro-expressing cells. HL-CZ cells were transiently co-transfected with plasmid pcDNA3.1 or pSARS-CoV 3CLpro plus a mitochondrial localization vector pDsRed-Mito (enhanced red fluorescent protein). After immunofluorescent staining, apoptosis-inducing factor and cytochrome c were probed by FITC–conjugated secondary antibodies. Confocal image analysis of the cells was performed using Leica TCS SP2 AOBS laser-scanning microscopy.

MHV RNA synthesis [40]. Therefore, the SARS-CoV 3CLpro that induced a significant increase in hnRNP expression could play an important role in coronavirus infection.

Interestingly, analysis of the apoptosis signaling pathway revealed that the mitochondrial apoptogenic apoptosis-inducing factor (Spot ID 55) was up-regulated and anti-apoptogenic heat shock cognate 71-kDa protein (HSP70) (Spot ID 83) was down-regulated in 3CLpro-expressing cells (Figs. 1, 2 and 6, Tables 1, 2 and 3). Apoptosis-inducing factor (Spot ID 55) was also released from the mitochondria of 3CLpro-expressing cells (Fig. 7A). Release of apoptosis-inducing factor from mitochondria results in a caspase-independent pathway of programmed cell death [41, 42]. Moreover, the other mitochondrial apoptogenic protein cytochrome c has been demonstrated to be released from mitochondria (Fig. 7B). Since the activation of caspase-3 and caspase-9 has been demonstrated previously to be involved in 3CLpro-inducing apoptosis [16], release of apoptosis-inducing factor and cytochrome c in the cytosol ise suggested to interact with apoptotic protease-activating factor 1 (Apaf-1) and dATP/ATP to activate apoptosome-mediated caspase-9 and process downstream effector caspases such as caspase-3. Therefore, the results reveal that SARS CoV 3CLpro induces mitochondrial-mediated apoptosis.

In conclusion, proteomic analysis of cellular responses to SARS CoV 3CLpro demonstrated that SARS CoV 3CLpro up-regulates the main biological process of protein metabolism and modification, particularly in the ubiquitin proteasome pathway. Moreover, the results showed that SARS CoV 3CLpro induces mitochondrial alternation in apoptosis signaling, electron transport and ATP synthesis. The study provides system-level insights into the interaction of SARS CoV 3CLpro with host cells, and is helpful for elucidating the molecular basis of SARS CoV pathogenesis.

We would like to thank China Medical University and National Science Council, Taiwan for financial supports (CMU95-152, CMU95-153, NSC94-2320-B-039-010 and NSC95-2320-B-039-019).

5 References

[1] Lee, N., Hui, D., Wu, A., Chan, P. *et al.*, *N. Engl. J. Med.* 2003, *348*, 1986–1994.

[2] Tsang, K. W., Ho, P. L., Ooi, G. C., Yee, W. K. *et al.*, *N. Engl. J. Med.* 2003, *348*, 1977–1985.

[3] Hsueh, P. R., Chen, P. J., Hsiao, C. H., Yeh, S. H. *et al.*, *Emerg. Infect. Dis.* 2004, *10*, 489–493.

[4] Nicholls, J. M., Poon, L. L., Lee, K. C., Ng, W. F. *et al.*, *Lancet* 2003, *361*, 1773–1778.

[5] Lang, Z., Zhang, L., Zhang, S., Meng, X. *et al.*, *Chin Med J (Engl).* 2003, *116*, 976–980.

[6] Ng, M. L., Tan, S. H., See, E. E., Ooi, E. E. *et al.*, *J Gen Virol.* 2003, *84*, 3291–3303.

[7] Yan, H., Xiao, G., Zhang, J., Hu, Y. *et al.*, *J Med Virol* 2004, *73*, 323–331.

[8] Mizutani, T., Fukushi, S., Saijo, M., Kurane, I. *et al.*, *Virology* 2004, *327*, 169–174.

[9] Lai, M. M. C., Holmes, K. V., *Fields Virology* 2001, 1163–1185

[10] Holmes, K. V., *Fields Virology* 2001, 1187–1203

[11] Ziebuhr, J., Snijder, E. J., Gorbalenya, A. E., *J. Gen. Virol.* 2000, *81*, 853–879.

[12] Anand, K., Ziebuhr, J., Wadhwani, P., Mesters, J. R. *et al.*, *Science* 2003, *300*, 1763–1767.

[13] Yang, H., Yang, M., Ding, Y., Liu, Y. *et al.*, *Proc. Natl. Acad. Sci. USA* 2003, *100*, 13190–13195.

[14] Lin, C. W., Tsai, F. J., Tsai, C. H., Lai, C. C. *et al.*, *Antiviral Res.* 2005, *68*, 36–42.

[15] Lin, C. W., Tsai, F. J., Wan, L., Lai, C. C. *et al.*, *FEBS Lett.* 2005, *579*, 6089–6094.

[16] Lin, C. W., Lin, K. H., Hsieh, T. H., Shiu, S. Y. *et al.*, *FEMS Immunol. Med. Microbiol.* 2006, *46*, 375–380.

[17] Kuyumcu-Martinez, N. M., Van Eden, M. E., Younan, P., Lloyd, R. E. *Mol. Cell. Biol.* 2004, *24*, 1779–1790.

[18] Neznanov, N., Chumakov, K. M., Neznanova, L., Almasan, A. *et al.*, *J. Biol. Chem.* 2005, *280*, 24153–24158.

[19] Chen, J. H., Chang, Y. W., Yao, C. W., Chiueh, T. S. *et al.*, *Proc. Natl. Acad. Sc. USA* 2004, *101*, 17039–17044.

[20] Jiang, X. S., Tang, L. Y., Dai, J., Zhou, H. *et al.*, *Mol. Cell. Proteomics* 2005, *4*, 902–913.

[21] Takashima, M., Kuramitsu, Y., Yokoyama, Y., Iizuka, N. *et al.*, *Proteomics* 2005, *5*, 1686–1692

[22] Cui, F., Wang, Y., Wang, J., Wei, K. *et al.*, *Proteomics* 2006, *6*, 498–504.

[23] Fang, C., Yi, Z., Liu, F., Lan, S. *et al.*, *Proteomics* 2006, *6*, 519–527.

[24] Wan, J., Sun, W., Li, X., Ying, W. *et al.*, *Proteomics* 2006, *6*, 2886–2894.

[25] Gharahdaghi, F., Weinberg, C. R., Meagher, D. A., Imai, B. S. *et al.*, *Electrophoresis* 1999, *20*, 601–605.

[26] Terry, D. E., Edward, U., Desiderio, D.M., *J. Am. Soc. Mass Spectrom.* 2004, *15*, 784–794.

[27] Hirosawa, M., Hoshida, M.,Ishikawa, M., Toya, T., *Comput. Appl. Biosci.* 1993, *9*, 161–167.

[28] Thomas, P. D., Campbell, M. J., Kejariwal, A., Mi, H. *et al.*, *Genome Res.* 2003, *13*, 2129–2141.

[29] Lazareva-Ulitsky, B., Diemer., K., Thomas, P. D., *Bioinformatics* 2005, *21*, 1876–1890.

[30] Mi, H., Lazareva-Ulitsky, B., Loo, R., Kejariwal, A. *et al.*, *Nucleic Acids Res.* 2005, *33*, D284–D288.

[31] Lee, I., Bender, E., Arnold, S., Kadenbach, B., *Biol. Chem.* 2001, *382*, 1629–1636.

[32] Roos-Mattjus, P., Sistonen, L., *Ann. Med.* 2004, *3*, 285–295.

[33] Yu, G. Y., Lai, M. M., *J. Virol.* 2005, *79*, 644–648.

[34] Shi, S. T., Yu, G. Y., Lai, M. M., *J. Virol.* 2003, *77*, 10584–10593.

[35] Galinier, R., Gout, E., Lortat-Jacob, H., Wood, J. *et al.*, *Biochemistry* 2002, *41*, 14299–14305.

[36] Gao, L., Tu, H., Shi, S. T., Lee, K. J. *et al.*, *J. Virol.* 2003, *77*, 4149–4159.

[37] Schubert, U., Ott, D. E., Chertova, E. N., Welker, R. *et al.*, *Proc. Natl. Acad. Sci. USA* 2000, *97*, 13057–13062.

[38] Li, H. P., Zhang, X., Duncan, R., Comai, L. *et al.*, *Proc. Natl. Acad. Sci. USA* 1997, *94*, 9544–9549.

[39] Li, H. P., Huang, P., Park, S., Lai, M. M., *J. Virol.* 1999, *73*, 772–777.

[40] Shi, S. T., Yu, G. Y., Lai, M. M., *J. Virol.* 2003, *77*, 10584–10593.

[41] Joza, N., Susin, S. A., Daugas, E., Stanford, W. L. *et al.*, *Nature* 2001, *410*, 549–554.

[42] Yu, S.W., Wang, H., Poitras, M. F., Coombs, C. *et al.*, *Science* 2002, *297*, 259–263.

